Supplement of

How combining multi-scale monitoring and compound-specific isotope analysis helps to evaluate degradation of the herbicide *S*-metolachlor in agro-ecosystems?

Boris Droz[1,•*], Guillaume Drouin[1,•], Jenna Lohmann[1], Benoit Guyot[1], Gwenaël Imfeld[1], Sylvain Payraudeau[1*]

[1] Institut Terre et Environnement de Strasbourg (ITES), University of Strasbourg/ENGEES, CNRS UMR 7063, France

• These authors contributed equally to this work.

[*]*Correspondence to*: Boris Droz (drozditb@oregonstate.edu) and Sylvain Payraudeau (sylvain.payraudeau@engees.unistra.fr)

Contents

S1 Supplement methods.

S1.1 Catchment and sub-catchment delimitation.

The European Digital Elevation Model (EU-DEM, v1.1, https://land.copernicus.eu) with a 25 m resolution for the year 2011, along with the river network data (BD TOPO® 2019, http://www.ign.fr), was used to delineate the catchment and sub-catchments (Kwast and Menke, 2022), using an automatic procedure implemented in GRASS v.7.2.2 within R4.2.2 (package 'rgrass' v.0.3-6) at both automated and grab sampling locations. Briefly, water flow direction was calculated for each pixel using a depression elevation map. Next, water accumulation was determined by counting the number of adjacent pixels that drain through each pixel. Finally, the catchment was delineated using the drainage direction and the sampling location, which serves as the catchment's outlet point.

S1.2 Catchment description and *S*-metolachlor application dose scenario.

For each agricultural field, three *S*-metolachlor application scenarios were considered: the maximum legal dose (hereafter 'maximal'), a dose based on local farming recommendations (https://alsace.chambre-agriculture.fr/, hereafter 'economic'; Table S1), and a dose derived from farmer surveys (hereafter 'realistic'). Application rates for each field were calculated using data from Table S1. Soils in the catchment areas (<20 m depth), as identified by satellite remote sensing, were predominantly Cambisols (83%), followed by Luvisols (13%), with the following predicted properties: bulk density 1.29 ± 0.04 kg dm^{-3}, clay 21.6 ± 1.9%, silt 45.9 ± 3.6%, and sand 32.5 ± 4.3% (Hengl et al., 2017).

Table S1: Main crop types and *S*-metolachlor application at the Souffel catchment in 2019.

Field	Crop type (%)[a]	*S*-metolachlor application (g ha^{-1} yr^{-1})		
		Maximal[b]	Economic[c]	Realistic min-max[d]
Sugar beet	10.4	576	384	576 – 672
Corn	49.7	1920	1280	160 – 1000
Wheat	21.9			
Others cereals	1.4		no application	
Meadow	4.6			
Vegetable (zucchini, pumpkin, squach, beans)	0.2	1500		not in survey
Soja / sorgho / sunflower	0.2	1344		
Divers (tabac, hops,…)	11.6		no application	

[a] Calculated from the Registre Parcellaire Graphique (www.ign.fr) from 2019. *S*-metolachlor applications are reported and then applied based on field type (https://ephy.anses.fr): [b] follow regulatory limits, [c] based on local farming recommendations (https://alsace.chambre-agriculture.fr/) and [d] based on survey results from the A2 sub-catchment.

Table S2: Sub-catchment characteristics.

Outlet of the catchment	A1	A2	A3
Size (km^2)	2.3	3.6	115
Slope (%)[a]	n.m.	3.8 ± 1.2	2.4 ± 2.2
River length (km)[a]	0.7	2.2	73
Strahler order[a]	1	1	1–3
Farmland (%)[a]	91	93	87
Prop. wheat/corn/beets (%)[b]	36/25/3	32/31/12	22/50/10
Prop. wheat/corn/beets (%)[c]	28/20/2	27/26/4	n.m.

[a] from BD TOPO® 2017, http://www.ign.fr/.

[b] Registre Parcellaire Graphique 2019, www.ign.fr.

[c] from survey.

n.m. not measured.

S1.3 Continuous sampling.

Table S3: Automatic water sampler characteristics, flow control and multiprobe devices.

Loc.	Sampling	Capacity (mL)	Flow slavering control	Flow meter	Temp., pH, cond.[a]
A1	ISCO Avalanche	12 x 350	Doppler (ISCO 2150)	ISCO 2150	Ponsel ODEON
A2	ISCO Avalanche	12 x 350	Doppler (IJINUS VLI H/V)	IJINUS VLI H/V	HANNA HI 9289
A3	ISCO 6712	24 x 950	Bubbler flow module (ISCO 730)	VEGAPULS WL S 61	HANNA HI 9289
G1–9	Grab sampling	2000	None	OTT Nautilus C2000 / Sensa Z300	WTW multi 350i

[a]Temperature, pH and conductivity were measured every two minutes.

Table S4: Rain gauge location and material.

ID	Name	Location (WGS 84)	Material	Accuracy (mm)	Ref.
R1	LYHGES	48°40'03"N 7°34'51"E	Precis Mecanique mouvement 3030	0.2	A
R2	IALSACES11	48°37'48"N 7°37'12"E	Davis Vantage Pro2 Plus	0.2	B
R3	EMSVENDEN	48°40'18"N 7°42'42"E	Precis Mecanique mouvement 3039/1	0.1	C
R4	EMSMUNDOL	48°38'25"N 7°43'16"E			C
R5	EMSOBERHAUS	48°36'20"N 7°41'46"E			C
R6	EMSWOLFIS	48°34'47"N 7°40'20"E			C
R7	EMSHOLTZ	48°33'47"N 7°39'00"E			C
R8	IWASSELO8	48°38'27"N 7°27'00"E	Eurochron EC-4406126	n.s.	B
R9	IALSACEC18	48°40'48"N 7°34'48"E	Davis Vantage Vue	0.2	B

A data is available in Droz et al. (2024), B data were downloaded from www.wunderground.com/weatherstation and C data are provide by the city of Strasbourg.

S1.4 Analytic methods.

Table S5: Analytic methods description.

Water characterization	Methods in brief	Reference
pH/conductivity/ temperature	Electrode measurement (pH/cond multi 350i, WTW).	
Water velocity	Handheld electromagnetic water flow meter (Nautilus C2000 / Sensa Z300, OTT).	
Total suspended solid (TSS)	Sample filtered with a bottle-top vacuum filtration unit through a glass filter (GF/5, 0.4 µm average pore size, Macherey-Nagel) and dried at room temperature in a dessicator.	Modified NF872
Bulk density	Weigh a soil field sample that has a cylindrical known volume (48 cm^3, core method).	ISO 11272
Dissolved organic carbon (DOC)/ dissolved inorganic carbon (DIC)	Sample is passed through a 0.25 µm cellulose acetate filter, then dissolved organic carbon is oxidized into CO_2 and detected by infrared spectrometry (TOC-V CPH, Shimadzu).	NF EN 1484
Iron (Fe^{2+}, Fe^{3+})	Presence/absence of iron is measured by semi-quantitative strip (P/N 1.16982.0001, Reflectoquant®, Merck) with reflectometer (P/N 1.16970.0001, Merck). If present, UV-vis spectrophotometric measurement is made at 511 nm after reaction with 1,10-phenanthroline to form a red complex (P/N 1.00796.0001, Spectroquant®, Merck).	DIN 38406-1
Cations/anions (Na^+, K^+, Mg^{2+}, Ca^{2+}, NH_4^+, Cl^-, NO_3^-, SO_4^{2-}, PO_4^{3-})	Ion chromatography analysis (ICS-5000, Dionex/Thermo Fischer). Bromide can be measured if there is a low sulfate content.	US EPA 300.7/300.0
Nitrite (NO_2^-)	Presence/absence of nitrite is measured by semi-quantitative strip (P/N 1.16973.0001, Reflectoquant®, Merck) with reflectometer (P/N 1.16970.0001, Merck). If present, UV-vis spectrophotometric measurement is made at 536 nm after Reaction with *N*-(1-naphthyl)ethylenediamine dihydrochloride to form a red-violet azo complex (P/N 1.14776.0002, Spectroquant®, Merck).	DIN 26777
Minor element (Mn, Cu, Si, Al, Fe, Zn, Ti, P)	Sample filtered through 0.25 µm, digest 1 mL sample by HNO_3 (50 mL, 69%) and oxalic acid (50 mL, 1 M), aqueous phase measured by inductively coupled plasma-optical emission spectrometry (ICP-OES, ICAP6500, Thermo Fisher).	In house method
Sediment characterization		
Residual humidity (RH) content	Sample dried until constant mass at 105°C.	ISO 11465
pH_{H2O}/ pH_{CaCl2}	Electrode measurement of 1:5 w/w sediment:water or 0.01 M $CaCl_2$.	ISO 10390
Organic carbon (f_{OC}) / inorganic carbon (C_{inorg})	Total combustion by elementary analyzer (CHN, FLASH 2000 NC, Thermo Fisher). Prior to organic carbon measurement, sample was decarbonated by HCl fumigation. C_{inorg} = total C - f_{OC}.	ISO 10694, Ramnarine et al. (2011)
Particle size fraction (0.1 µm to 2 mm)	Sample was pre-treated with a proportion 1:3 (v/v) of H_2O_2 at 60 °C to degrade organic matter, KCl 1:50 (v/v) or HCl 1:20 (v/v) was added if the sample contained carbonate or no carbonate respectively to extract flocculent cations and 1:1 (v/v) solution of Natrium hexametaphosphate 0.55% was added to disperse the particles. Measurement performed by laser granulometer in aqueous mode (LS230, Beckmann Coulter).	ISO 13320
Elementary analysis (Na, K, Mg, Ca, Ti, Mn, Fe, AI, Si)	Sample prepare by fusion alkaline with lithium tetraborate and analysed by inductively coupled plasma-optical emission spectrometry (ICP-OES, ICAP6500, Thermo Fisher).	NF ISO 14869-2

The minimal change of isotope signature of the ^{13}C ($\Delta\delta^{13}C_{min}$), before which isotope fractionation can be attributed to degradation, was determined as the propagation of uncertainties associated with measurements and sample preparation (Alvarez-Zaldívar et al., 2018) and calculated as follow:

$$\Delta\delta^{13}C_{min} = \sqrt{\sigma_{ea}^2 + \sigma_s^2 + \sigma_{au}^2} + \Delta\delta^{13}C_{ext} \quad \text{(S1)}$$

where $\sigma_{ea}^2, \sigma_s^2$ and σ_{au}^2 are the uncertainty associated with the triplicate measurement of the initial product by an elemental analyzer IRMS (0.5‰ for C), the sample uncertainty associated with the triplicate measurement and the maximal analytical uncertainty of the GC-IRMS (0.5‰ for C), respectively. $\Delta\delta^{13}C_{ext}$ (−1.23 ± 0.3‰ and 0.11 ± 0.4‰ for sediment and water respectively) is the trueness of the $\delta^{13}C$ measurement associated with the extraction procedure, as previously determined in Droz et al. (2021).

S1.5 *S*-metolachlor mass balance.

S1.5.1 Estimation of the volatilization after application.

Proportion of volatilization after application was estimated based on the semi-empirical physical based model developed from Hippelein and Mclachlan (2000) and generalized over 224 molecules including *S*-metolachlor by Davie-Martin et al. (2013). Briefly, the model relies on a multiphase partitioning approach based on soil−air ($K_{soil-air}$) and water−air ($K_{water-air}$) partition coefficients for the topsoil. Air temperature and moisture combined with topsoil relative moisture and organic carbon content are the principal parameters accounting for variation of the rate of the volatilization in the model, which was consistent with observations made in agricultural fields (Gish et al., 2011; Prueger et al., 2005). The volatilization was only considered to take place for 36 h following application as observed in the field (Gish et al., 2011; Prueger et al., 2005). Table S6 summarizes the parameter values used in the model to calculate the volatilization after each reported application. The predicted contribution of volatilization accounts for 2.2 to 5.5% mass loss of applied *S*-metolachlor within 36 h after the application, which is consistent with the [^{14}C]metolachlor experiment on unsaturated subsurface soils where volatilization was less than 5% (Rice et al., 2002).

Table S6: Local parameters used for the volatilization estimation.

Parameter	Values	Reference
Temperature (min–max)	5.7–20.9°C	www.meteo-offenheim.fr
Relative humidity (annual average)	77%	www.meteo-offenheim.fr
Bulk density	1.29 kg L^{-1}	Hengl et al. (2017)
Soil organic carbon	0–50%	Hengl et al. (2017)
Soil depth[a]	50 cm	Huang and Frink (1989)
Soil moisture	min–max 0–100% average: 28%	Bauer-Marschallinger et al. (2018)

[a] topsoil depth average where >80% of the *S*-metolachlor total amount in topsoil was found within 1-2 weeks following application.

S1.5.2 Estimation of photodegradation in the Souffel river.

The extent of *S*-metolachlor photodegradation was estimated as following in Fono et al. (2006) and Schwarzenbach et al. (2016). Briefly, the ratio of day-average surface solar intensities L(330 nm) measured during solar simulating photodegradation experiments (Drouin et al., 2021) and the Souffel River were estimated from the Greifensee (Switzerland, 47°21'59"N 8°39'42"E) (Leifer, 1988) using the following constant:

Solar simulator: $L_{sim}(330nm) = 6.05\times10^{-2}$ mE cm^{-2} day^{-1}

Souffel River: $L_{river}(330nm) = 4.34\times10^{-2}$ mE cm^{-2} day^{-1}

Then, the depth of the photic zone in the Souffel River and the photic zone is defined as follows:

$$A = \log(I_0/I) = 1.3 \quad \text{(S2)}$$

where A was the absorbance and I the intensity, respectively.

$$A_{330nm} = \alpha_{330} \times Z_{photic} \quad \text{(S3)}$$

where α_{330} was the beam attenuation coefficient (6 m^{-1} for muddy river water) and Z_{photic} the depth of the photic zone.

$$S = \frac{(1-e^{-\alpha_{330}\times Z_{photic}})}{\alpha_{330}\times Z_{photic}} \quad \text{(S4)}$$

where S was the screening factor to account for DOM sorption.

$$k_{phot,river} = \frac{k_{phot,sim}}{L_{sim}/L_{river}} \times S \quad \text{(S5)}$$

where $k_{phot,river}$ and $k_{phot,sim}$ were the photodegradation rate in the river and the photodegradation rate during the solar simulating photodegradation under nitrate conditions. $k_{phot,sim}$ under nitrate conditions ($k_{phot,sim}$ = (1.3 ± 0.1) × 10^{-6} s^{-1}) could be considered to be the maximum photodegradation because no dissipation by dissolved organic matter was taken into account (Drouin et al., 2021). Hence, photodegradation rates might be slightly overestimated.

S1.6 Variation of *S*-metolachlor concentrations in topsoil.

During the 2019 campaign, *S*-metolachlor concentrations in topsoil were measured, although the associated $\delta^{13}C$ values could not be measured due to matrix effects. Therefore, $\delta^{13}C$ was estimated from measured *S*-metolachlor concentrations in topsoils, as validated in a similar agricultural headwater catchment (Payraudeau et al., 2024). Briefly, *S*-metolachlor biodegradation in topsoil is calculated from a corrected first-order constant (k_{dyn}) accounting for the observed topsoil temperature (T_{obs}) and moisture (θ_{obs}), as follows in Boesten and Linden (1991):

$$k_{dyn} = k_{Ref} \times f_T \times f_\theta \quad \text{(S6)}$$

where f_T and f_θ are the factors that account for the influence of the topsoil temperature and moisture (w/w). The factors for the influence of topsoil temperature follow the Arrhenius laws as follows in Walker (1974):

$$f_T = \begin{cases} 0 & \text{if, } \mathrm{T_{obs}} \leq \mathrm{T_{ref}} \\ \frac{T_{obs} - \mathrm{T}_{ref}}{5} \times e^{\frac{E_a}{R} \times \left(\frac{1}{T_{ref}} - \frac{1}{T_{obs}}\right)} & \text{if, } \mathrm{T_{ref}} < \mathrm{T_{obs}} \leq (\mathrm{T_{ref}} + 5) \\ e^{\frac{E_a}{R} \times \left(\frac{1}{T_{ref}} - \frac{1}{T_{obs}}\right)} & \text{if, } \mathrm{T_{obs}} > (\mathrm{T_{ref}} + 5) \end{cases} \quad \text{(S7)}$$

where T_{ref} is the reference temperature (293.15 K) in Kelvin, E_a is the *S*-metolachlor activation energy (2.391×10^3 J mol^{-1}) and R is the gas constant (8.314 J mol^{-1} K^{-1})(Jaikaew et al., 2017).

The relation to soil moisture follows (Walker, 1974):

$$f_\theta = \left(\frac{\theta_{obs}}{\theta_{ref}}\right)^{\beta_\theta} \quad \text{(S8)}$$

where β_θ is a calibration constant and θ_{ref} the reference water content, which was set at 0.5 and 0.2, respectively. θ_{obs} and T_{obs} for the growing season were obtained for the 0–20 cm topsoil at a 8 km spatial resolution for the year 2019 by the national weather service (https://publitheque.meteo.fr) computed by a daily soil water budget model (Habets et al., 2008).

Initial *S*-metolachlor concentrations in topsoil were estimated from application rates reported in the farmer surveys. *S*-metolachlor doses were assumed to be present within the top 10 cm of topsoil (Silva et al., 2019). Bulk soil density was set at 1.29 kg dm^{-3} according to the soilgrid data for the agricultural area within the catchment (Hengl et al., 2017).

Isotope fractionation was predicted from the *S*-metolachlor biodegradation in topsoil using a Rayleigh equation,

$$ln\left(\frac{\delta^{13}C(t)+1}{\delta^{13}C_0+1}\right) = \varepsilon_{bulk,C} \times ln\left(\frac{P(t)}{P_0}\right) \quad \text{(S9)}$$

where $\delta^{13}C_0$ and $\delta^{13}C(t)$ represent the isotope signatures of the carbon at time zero and time t of degradation respectively, while $P(t)/P_0$ is the fraction of remaining pesticides at time t. Considering $\varepsilon_{bulk,C}$ = –1.4 ± 0.4‰ determined in Droz et al. (2021) and the $\delta^{13}C_0$ as the signature from the commercial product (Table S7) (Alvarez-Zaldívar et al., 2018).

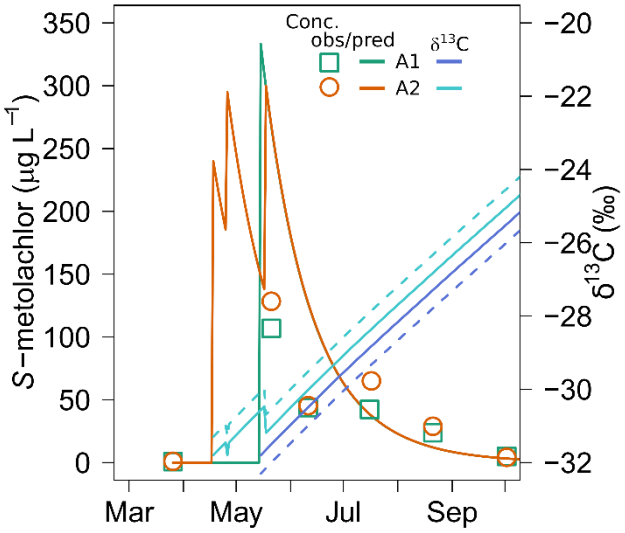

Figure S1: Measured and predicted *S*-metolachlor topsoil concentrations at A1 and A2 (Fig. S2). Colored dashed lines represent the predicted uncertainty of the topsoil $\delta^{13}C$ estimated as the minimum ± 0.5‰.

Table S7: Carbon stable isotope signatures ($\delta^{13}C$) of commercial products containing *S*-metolachlor.

Commercial name	δ^{13}C (‰)			*n*
Dual Gold[a]	–31.9	±	0.2	4
Camix[a]	–31.7	±	0.2	4
Mercantor Gold[a]	–31.3	±	0.2	4
Mercantor Gold[b]	–32.2	±	0.5	3
S-Metolastar[a]	–32.1	±	0.2	5
average	**–31.8**	**±**	**0.3**	

Uncertainties correspond to the SD from *n* measurements.
Measured in [a] this study and [b] Alvarez-Zaldívar et al. (2018)

S1.7 Piezometer description

Three piezometers were installed on 19 September 2019, at a distance of 2.5 m from the banks of the Avenheimerbach (Fig. S2). Piezometers PZ1 and PZ2 were positioned 2 m upstream of sampling point A2, on the right and left banks, respectively. PZ3 was located 35 m downstream of sampling point A1 on the left bank. Each piezometer was 3 m deep and constructed from PVC tubing (SDEC, Reignac-sur-Indre, France), with slotted sections over the bottom 2 m (Fig. S2). All piezometers were equipped with integrated OTT CTD sensors and data loggers (OTT, Kempten, Germany) to monitor water level, temperature, and conductivity, with an accuracy of 0.05%.

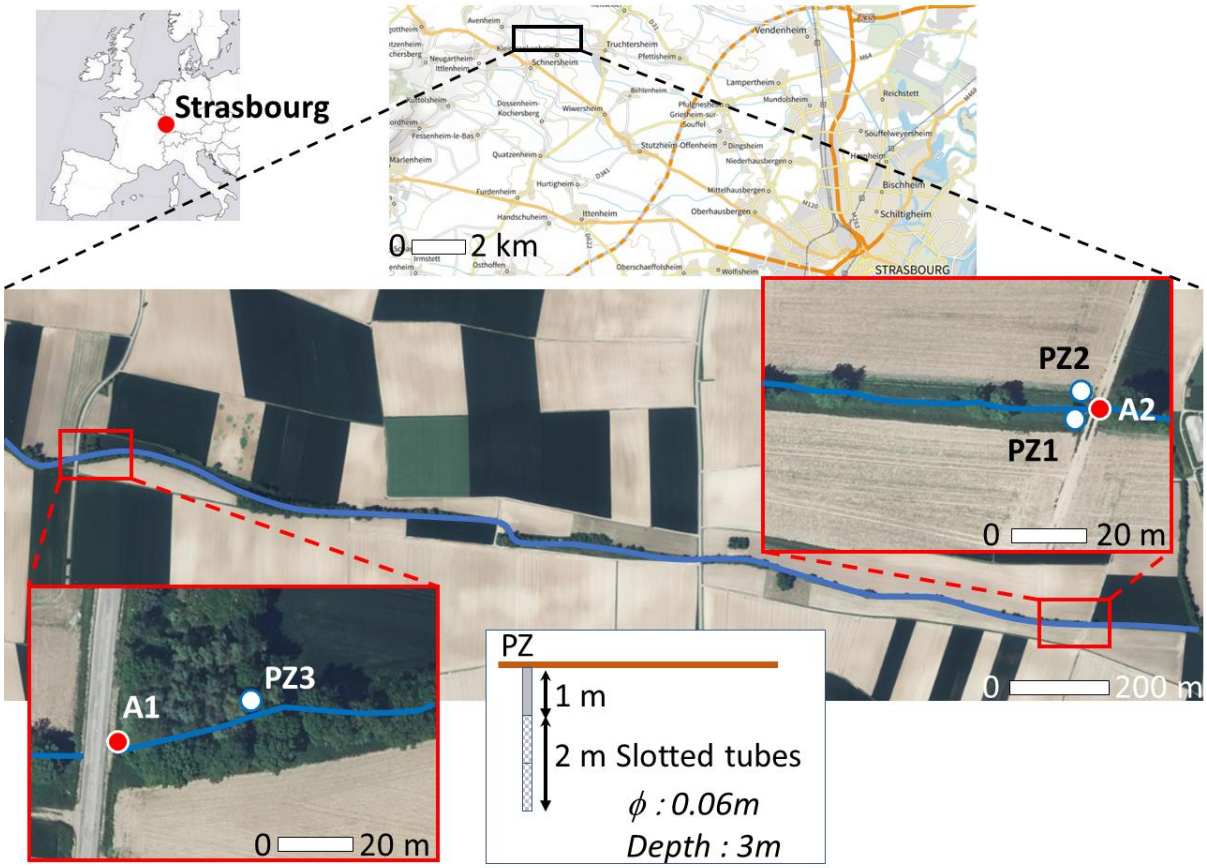

Figure S2: Location of the 3 piezometers on the Avenheimerbach river (Souffel catchment, France, BD ORTHO® | Géoservices - IGN).

S1.8 Averaged transit time and degradation within the river reach between A1 and A2.

Considering no retardation effects in accordance with limited interactions of *S*-metolachlor with the sediment riverbed (Lemke et al., 2013), the average transit time of dissolved *S*-metolachlor within the river reach in between A1 and A2 (Fig. S2) is assumed to be similar as the water travel time. A V-shape channel geometry of average width 6.5 m and depth 1.5 m (m = 6.5/1.5 = 4.3 the channel bank slope) can be considered as representative of the whole river reach. Under uniform and steady state conditions, the normal velocity in the river can be estimated with the Manning-Strickler relationship (Akan, 2006) as follow:

$$Q_n = K_s \times S \times n \times R_h^{2/3} \times \sqrt{I} \quad \text{(S10)}$$

where Q_n refers to the normal velocity in m^3s^{-1}, K_s to the Strickler coefficient in $m^{1/3}s^{-1}$ and is equal to $K_s = 1/n$, n the Manning's roughness coefficient (n for clay river beds is 0.030 (Akan, 2006)), R_h to the hydraulic radius in m defined as $R_h = S/P$ with S the cross-sectional area in m^2 and P the wetted perimeter in m, and I to the average channel slope (I = 1.1%). Under low-flow conditions, with the average water flow rate between A1 and A2 ranging from 5 to 10 × 10^{-3} m^3 s^{-1}, the normal water height (h_n) can be determined to be between 6 and 8 cm within the channel, based on the numerical application of Eq. S10. Thus, applying Eq. S11, the average velocity (v_n) under low flow conditions is estimated between 33 and 40 cm s^{-1}. Finally, considering the total length of the

A1−A2 river reach of 2.2 km, under low flow conditions, *S*-metolachlor transit time within the A1−A2 river reach is estimated between 1.4 and 1.7 hours.

$$Q_n = \frac{v_n}{S} = \frac{v_n}{m \times h_n^2} \quad \text{(S11)}$$

S1.9 Stable isotope fractionation with increasing *S*-metolachlor transit time.

Despite the negligible isotope fractionation observed in the sub-catchment A1−A2, CSIA may prove useful for larger rivers displaying significantly longer transit time. Considering no retardation effects in accordance with limited interactions of *S*-metolachlor with the sediment riverbed (Lemke et al., 2013), the equivalent transit time (t_{eq}) of dissolved *S*-metolachlor within the river reach is considered to be equal to the water travel time follow:

$$t_{eq} = \frac{v_{water}}{L_{water}} \quad \text{(S12)}$$

where v_{water} and L_{water} being the overlying water velocity and the river length respectively. Using laboratory derived degradation rates, it is possible to estimate the *S*-metolachlor equivalent transit time above, which can be used with CSIA data to quantify degradation extent instream. The laboratory derived photodegradation (Drouin et al., 2021) and biodegradation (Droz et al., 2021) half-lives of *S*-metolachlor of 6 and 30 days and isotopic enrichment factors of $\varepsilon_{bulk,N}$ = −0.7 ± 0.4‰ for photodegradation and $\varepsilon_{bulk,C}$= −1:2 ± 0.4‰ for biodegradation were considered. As photodegradation and biodegradation co-occur in rivers, the Rayleigh Eq. (S9) was corrected according to Van Breukelen (2007) Eq. (S13):

$$\varepsilon_{eff} = \frac{k_{photo} \times \varepsilon_{photo} + k_{biodeg} \times \varepsilon_{biodeg}}{k_{photo} + k_{biodeg}} \quad \text{(S13)}$$

with $\varepsilon_{eff}$the effective isotopic enrichment factor to be re-injected in Eq. (5) to define the extent of biodegradation. Accordingly, for *S*-metolachlor, isotope fractionation in C higher than the threshold of $\Delta\delta^{13}C_{min}$ = 2.0 ‰ is required to reliably confirm the occurrence of *S*-metolachlor degradation in rivers with a minimal water transit time higher than 800 hours.

However, for longer river reaches the retardation caused by interactions with the riverbed sediment, i.e., contaminant penetration and sorption into the sediment or instream vegetation, may further exacerbate instream degradation. Although retardation factors are very case- and molecule-specific a higher-bound value of two may be considered for testing the potential of CSIA to quantify instream degradation over long rivers (Liao et al., 2013; Salehin et al., 2003). Consequently, a minimal water transit time of 400 h (17 days) should be achieved to measure a significant $\Delta\delta^{13}C_{min}$. No equivalent river length was expressed as long equivalent transit times like this one correspond to high Strahler order rivers with flows and velocities varying at each confluence.

S2 Supplement results.

S2.1 Area-normalized discharges.

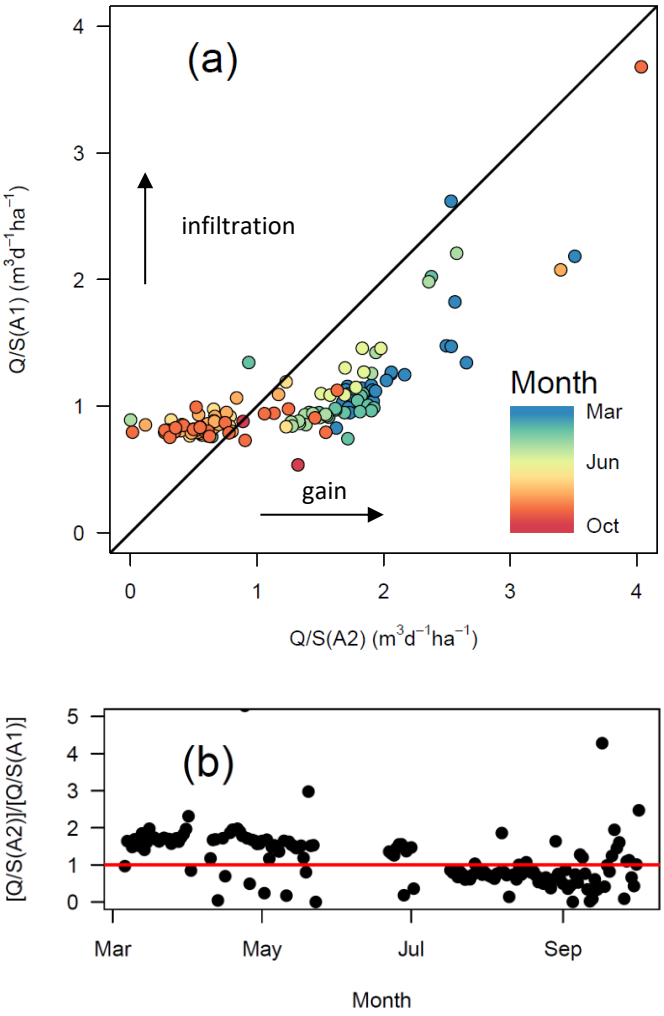

Figure S3: Area-normalized daily discharges in A1 vs A2. (a) Area-normalized daily discharges of A1 as a function of A2. The black line represents the 1:1 line. Area-normalized daily discharges at the beginning of the monitoring period range from blue to bright yellow. Colours get increasingly red later in the season, indicating a change from strong to light groundwater upwelling fluxes entering the A1–A2 river reach. (b) Area-normalized daily discharge ratios between A1 and A2.

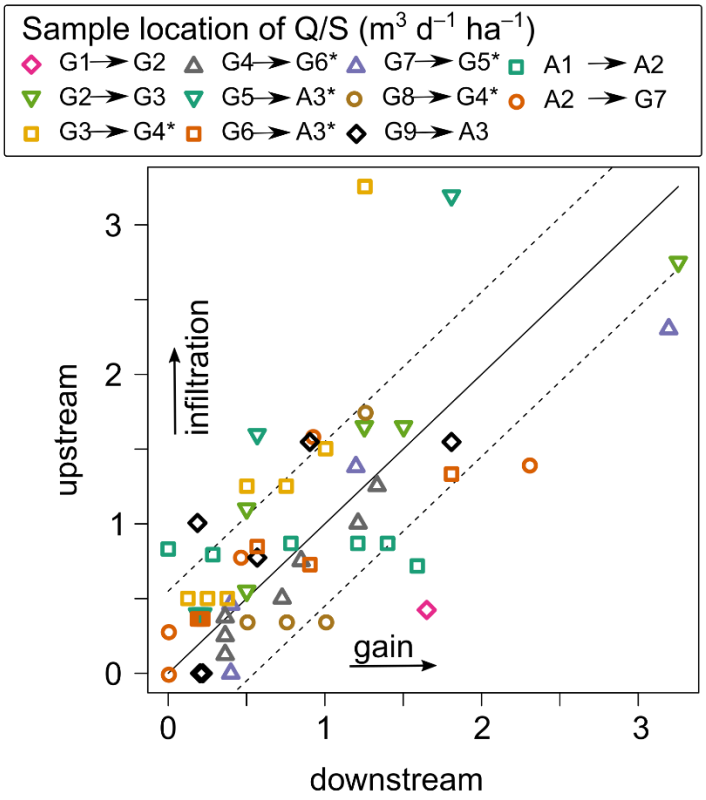

Figure S4: Upstream and downstream normalized flow (Shaw et al., 2019) i.e., discharge divided by surface of the corresponding sub-catchment, for all grab sampling events. Solid line indicates a 1:1 relationship and dashed line the 95% confidence interval considering a measured flow with 30% uncertainty. Asterisks (*) highlight reaches with WWTP contribution.

S2.2 Wetness index.

Topographical wetness index (TWI) was used to identify contributing areas prone to generate overland flow (Ali et al., 2014) and is computed as follows:

$$TWI = ln(a/\tan(b)) \quad \text{(S14)}$$

where a is the upslope area draining through a certain point per unit contour length and tan(b) is the local slope in radians. The catchment has a very low TWI (6.5 ± 1.4 ($\bar{x}$ ± SD)) with only 7.5% of the riverbank associated with a TWI higher than 8.5, which suggests that only a limited area likely contributed to overland runoff (Fig. S4). The EU-DEM 2011 was used to calculate TWI using SAGA-GIS 2.3.2+ through RSAGA package v1.3.0.

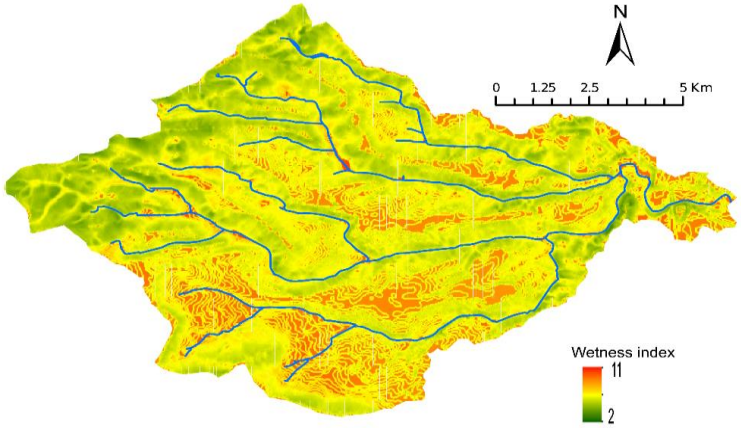

Figure S5: Topographical wetness index (TWI) of the Souffel catchment.

S 2.3 *S*-metolachlor concentrations per location.

Table S8: *S*-metolachlor mean concentrations ($\bar{x}$), standard deviation (SD), minimal and maximal concentration (min–max), frequency of the detection (freq.) and number of samples investigated (n) per location during the sampling period.

	dissolved *S*-metolachlor (µg L^{-1})				particulate *S*-metolachlor (µg kg^{-1})			sediment *S*-metolachlor (µg kg^{-1})			
	$\bar{x}$ ± SD (min–max)		freq. (%)	n.	$\bar{x}$± SD (min–max)	freq. (%)	n.	$\bar{x}$ ± SD (min–max)		freq. (%)	n.
continuous samples at the outlet											
A1	0.74 ± 2.22	(0.02–14.3)	86	58	< LD	0	9	6.79 ± 7.18	(1.72–11.9)	29	7
A2	0.48 ± 0.80	(0.02–5.37)	96	69	< LD	0	24	2.47	(2.46)	13	8
A3	2.24 ± 7.11	(0.03–54.6)	96	67	< LD	0	35	3.48	(3.48)	17	6
A1–3	**1.18 ± 4.47**	**(0.02–54.6)**	**93**	**194**	**< LD**	**0**	**68**	**4.88 ± 4.71**	**(1.72–11.9)**	**19**	**21**
grab samples											
G1	0.14 ± 0.25	(0.02–0.59)	71	7	< LD	0	2	< LD		0	1
G2	3.69 ± 8.71	(0.02–21.5)	86	7	< LD	0	2	< LD		0	7
G3	0.32 ± 0.42	(0.06–0.94)	57	7	< LD	0	1	< LD		0	7
G4	0.99 ± 1.15	(0.14–2.66)	57	7	< LD	0	4	< LD		0	7
G5	0.26 ± 0.16	(0.10–0.51)	71	7	< LD	0	1	7.38 ± 3.01	(5.26–9.51)	29	7
G6	0.82 ± 1.12	(0.03–2.73)	71	7	< LD	0	4	5.15	(5.15)	14	7
G7	0.09 ± 0.04	(0.02–0.13)	71	7	n.m.			< LD		0	7
G8	0.17 ± 0.21	(0.03–0.41)	75	4	< LD	0	1	< LD		0	5
G9	0.98 ± 1.78	(0.09–4.16)	71	7	< LD	0	3	6.09	(6.09)	14	7
G1–9	**0.94 ± 3.35**	**(0.02–21.5)**	**72**	**60**	**< LD**	**0**	**18**	**6.5 ± 2.0**	**(5.15–9.51)**	**7**	**55**
all river samples											
A1-G9	**1.13 ± 4.28**	**(0.02–54.6)**	**88**	**254**		**0**	**86**	**5.69 ± 3.47**	**(1.72–11.9)**	**11**	**76**
grab wastewater treatment plant (WWTPs) samples											
W1	0.40 ± 0.54	(0.01–1.28)	100	7	n.m.			n.m.			
W2	0.30 ± 0.32	(0.01–0.96)	100	7	< LD	0	2	n.m.			
W3	8.9 ± 20.2	(0.26–50.2)	86	7	< LD	0	2	n.m.			
W1-3	**2.9 ± 11.1**	**(0.01–50.2)**	**95**	**21**	**< LD**	**0**	**4**	**n.m.**			

	S-metolachlor (µg kg^{-1})			
soil samples	$\bar{x}$ ± SD (min–max)		freq. (%)	n.
A1	37.1 ± 38.6	(0.82–107)	100	6
A2	45.5 ± 47.4	(0.99–128)	100	6

n.m. not measured, < LD below limit of detection which is 1.2 µg kg^{-1}.

S 2.4 Detailed off-site transport of *S*-metolachlor per events

Over 9% of the seasonal *S*-metolachlor export (Events 1 and 2; Table S9) occurred before the first recorded applications. This early export cannot be fully explained by residual topsoil *S*-metolachlor from the previous year, which the mass balance (Table S10) estimated to contribute only 0.8–1.5% of the seasonal load. Events 8 and 12 triggered sharp increases in *S*-metolachlor concentrations, reaching approximately 5 $\mu g\,L^{-1}$ at sites A1 and A2. These events accounted for 17.5% and 29.5% of the total export at A1 and A2, respectively. Although runoff was considered unlikely during Event 12, its cumulative rainfall (36 mm)—the highest of the season—may have induced localized surface runoff.

Subsurface flow during moderate rainfall events (excluding Events 8 and 15) also contributed significantly, representing 28.5% and 70.5% of the total load at A1 and A2, respectively. While intense rainfall events caused the largest individual exports, subsurface transport played a dominant role over time. A single rainfall event on May 18, just two days after *S*-metolachlor application on corn, was responsible for 54% of the total seasonal export at A1, with a peak concentration of 14.33 $\mu g\,L^{-1}$. This export likely occurred via lateral subsurface flow, consistent with transport patterns during other moderate post-application rainfall events (10–16 $mm\,h^{-1}$) (Lefrancq et al., 2017). Flash export in clayey soils by preferential flows in soil cracks may also explain the transient character of this event, as described for bentazone and MCPA (2-methyl-4-chlorophenoxyacetic acid) and other pesticides (Kronvang et al., 2004).

Table S9: *S*-metolachlor concentrations and load dynamics at the outlet of the Souffel catchment for the main rainfall events (export of 91% of the seasonal load).

Event	1+2	3[b]	4	5	6[b]	7
Duration (hours)[a]	99 ± 24	101	80 ± 4	7 ± 6	1	42 ± 53
Amount (mm)[a]	28 ± 14	11	26 ± 9	11 ± 8	2.6	18 ± 14
Days since last application (d)	p.a.	8[c]	20[d]	15[e]	17[e]	21[e]
Mass applied (kg)[f]	0 (%)	160 ± 6 (5%)	319 ± 12 (10%)	3163 ± 116 (100%)		
Max con. ($\mu g\,L^{-1}$)	2.56	1.51	1.45	6.28	0.07	3.10
Load (kg)[g]	0.44 (9%)	0.57 (12%)	0.44 (9%)	2.28 (47%)	0.44 (9%)	0.29 (5%)
Max flow ($m^3\,s^{-1}$)	0.85	0.28	0.61	2.20	0.14	0.61

[a] considers rainfall gages R1, R2 and R9 only, [b] rainfall event detected only in R1, [c, d, e] considers application dates of April 18, April 29 and May 20, 2019, respectively, according to the survey of sub-catchment A2 (Section S1.1). [f] accounts for the realistic scenario (Table S1), percent of the total mass applied in parentheses, [g] loads corresponding to the rainfall event, percent of the total load in parentheses. p.a. pre-application. Average flow discharge is 0.115 $m^3\,s^{-1}$.

S2.5 Pesticide mass balance

A seasonal mass balance of *S*-metolachlor at the catchment scale—from application through October—was established using data from laboratory experiments, field observations, and river monitoring (Eq. 3; Table S10). At the field scale, volatilization was modeled based on soils, climate, and crop types comparable to those in the

study area (Table S6), suggesting that 2.2–5.5% of the applied *S*-metolachlor volatilized within one day of application. Prior to this study, off-site transport of *S*-metolachlor from agricultural topsoil to surface and groundwater at the catchment scale was poorly quantified. Monitoring results showed that this transport accounted for less than 1% of the applied mass in the upstream reach (A1–A2), and less than 0.1% at the full catchment scale in 2019.

Due to short water residence times, in-river biodegradation was limited, with an estimated contribution of $2.7 \pm 2.3\%$ (mean ± SD). Additional degradation processes included 0.3% at the sediment–water interface under anoxic conditions and 10% via photolysis in the water column, both estimated using first-order kinetics and representing point and non-point sources. The *S*-metolachlor load measured at the catchment outlet represented only 0.05–0.1% of the total applied amount. The mass balance closed within a 2% margin of error and indicated that $98.9 \pm 4.7\%$ of the applied *S*-metolachlor was degraded during the season, accounting for uncertainties in application scenarios.

This balance, supported by monthly concentration data from topsoil, river water, and WWTP effluents, and by continuous load monitoring at the outlet, was compared with degradation estimates from monthly CSIA measurements. As *S*-metolachlor does not exhibit isotope fractionation under photolysis, CSIA results reflect biodegradation exclusively (Drouin et al., 2021). In October, biodegradation estimates derived from CSIA and mass balance were in strong agreement, yielding values of $98 \pm 20\%$ and $98.9 \pm 4.7\%$ (mean ± SD), respectively. While CSIA exhibited higher analytical uncertainty, its advantages include minimal data requirements, contrasting with the extensive sampling and multiple assumptions required to establish a catchment-scale mass balance.

Table S10: Mass balance at the catchment scale A3 in the agricultural field and river.

	Unit	$\bar{x}$ ± SD (min–max)
Catchment area	km^2	120
Application area[a]	km^2	64.5 ± 2.2
S-metolachlor application and stock in the soil		
Stock in the soil (top 10 cm) before applications[b]	kg	7.49 ± 0.26
Maximal scenario	kg	8919
Economic scenario	kg	5969
Realistic scenario (survey)	kg	3163 ± 116
Stock in the soil (top 10 cm) after 214 days[b]	kg	38.2 ± 1.3
Hydrology[c]		
Outflow discharge (0−214 days)	$m^3\ day^{-1}$	8800 ± 9050 (1400–72,270)
Erosion[c]		
TSS export (0−214 Days)	t	720
S-metolachlor export in runoff/discharge[c]		
Dissolved export (0−214 days)	kg	4.87 ± 1.00
Particulate export (0−214 days)	kg	n.o.
Total export (dissolve and particulate) (0−214 days)[d]	%	(0.04 – 0.19)
WWTP *S*-metolachlor load[e]	%	49 ± 6
	kg	2.4 ± 0.8
Dissipation process in the river stretch		
Sorption in sediment bed		n.o.
Hydrolysis (0−214 days)		n.o.
Hyporheic exchange		n.m.
Photolysis (0−214 days)	%	10.4 ± 2.9
	g	506 ± 23
River biodegradation (0−214 days)	%	2.7 ± 2.3
	g	131 ± 20
Dissipation process at the catchment		
Volatilization (0–36 h after application)	%	(2.2 – 5.5)
Total biodegradation (0–214 days)	**%**	**98.9 ± 4.7**
(account for all degradation process)	**kg**	**(4740 – 9337)**
Remaining mass unaccounted for[d]	kg	(91 – 142)
	%	1.50 – 1.90

[a] calculated based on Table S1. [b] extrapolated from the topsoil data in the vicinity of A1 and A2 (n = 2). [c] data from the outlet of the catchment (n = 67), [d] range covered by the three scenarios. [e] estimated from grab sampling (n= 7 x 3 locations). n.o. not occuring, n.m. not measured.

S2.6 Hydrochemistry

Significant differences were observed between river (A1-3 and G1-9) and WWTP (W1-3) outlet samples, with higher chloride, sodium and potassium concentrations observed in the WWTP outlets (Tukey's test; p <0.01). Conversely, nitrate concentrations in the river ($\bar{x}$ ± SD = 41.2 ± 18.4 mg L^{-1}; n = 84; Table S11) were higher than those at the WWTP outlets (p <0.01; $\bar{x}$ ± SD =16.2 ± 18.0 mg L^{-1}; n = 21; Table S11). This indicates that a significantly larger proportion of nitrate comes from non-point sources versus WWTP effluent.

Table S11: Water composition during grab sampling at each location ($\bar{x}$ ± SD; n = 7 per location).

loc.	pH (-)	cond. (mS cm^{-1})	T (°C)	TSS (mg L^{-1})	DOC (mg L^{-1})	NH_4^+ (mg L^{-1})	Na^+ (mg L^{-1})	K^+ (mg L^{-1})	Mg^{2+} (mg L^{-1})	Ca^{2+} (mg L^{-1})	Cl^- (mg L^{-1})	NO_3^- (mg L^{-1})	SO_4^{2-} (mg L^{-1})	HCO_3^- (mg L^{-1})	CO_3^{2-} (mg L^{-1})
G1	9.0 ± 0.7	0.931 ± 0.023	14.2 ± 2.2	105 ± 102	1.54 ± 0.48	0.00 ± 0.00	6.8 ± 0.4	2.4 ± 0.3	56 ± 2	130 ± 14	26 ± 2	56 ± 2	169 ± 18	301 ± 114	53 ± 45
G2	8.5 ± 1.1	1.190 ± 0.122	16.4 ± 3.2	82 ± 112	1.87 ± 0.54	0.08 ± 0.16	10.5 ± 1.4	4.9 ± 0.6	41 ± 5	185 ± 24	31 ± 4	41 ± 5	364 ± 58	326 ± 103	41 ± 62
G3	8.9 ± 0.8	1.057 ± 0.301	16.5 ± 3.1	181 ± 197	3.58 ± 1.92	0.34 ± 0.77	25.6 ± 34.5	8.0 ± 7.3	34 ± 16	143 ± 53	51 ± 30	34 ± 16	231 ± 116	320 ± 92	71 ± 90
G4	8.1 ± 0.5	1.165 ± 0.104	13.3 ± 3.9	580 ± 708	5.83 ± 5.26	10.35 ± 7.37	29.1 ± 9.9	8.7 ± 2.0	26 ± 7	158 ± 9	53 ± 6	26 ± 7	234 ± 47	382 ± 117	57 ± 122
G5	8.2 ± 0.5	0.900 ± 0.162	14.1 ± 3.4	136 ± 93	4.91 ± 1.14	0.38 ± 0.49	54.2 ± 22.9	12.3 ± 4.5	37 ± 13	111 ± 29	89 ± 33	37 ± 13	75 ± 11	383 ± 109	11 ± 14
G6	7.8 ± 0.4	1.061 ± 0.157	13.0 ± 3.9	784 ± 976	6.97 ± 6.62	7.77 ± 5.57	43.9 ± 16.8	11.8 ± 3.8	24 ± 9	132 ± 16	71 ± 20	24 ± 9	181 ± 29	397 ± 85	4 ± 5
G7	8.3 ± 0.5	0.837 ± 0.339	14.7 ± 2.8	108 ± 167	2.87 ± 0.53	0.67 ± 1.26	20.0 ± 4.9	4.1 ± 1.5	52 ± 11	140 ± 18	61 ± 7	52 ± 11	81 ± 9	443 ± 72	19 ± 27
G8	8.5 ± 0.3	0.831 ± 0.044	15.0 ± 3.9	149 ± 222	3.62 ± 0.55	0.53 ± 0.98	27.0 ± 3.4	8.1 ± 3.3	31 ± 4	114 ± 18	66 ± 8	31 ± 4	77 ± 10	371 ± 65	16 ± 10
G9	8.4 ± 0.4	1.076 ± 0.066	14.2 ± 3.6	57 ± 51	5.25 ± 4.96	0.19 ± 0.34	36.1 ± 40.2	8.2 ± 5.2	35 ± 15	158 ± 46	78 ± 52	35 ± 15	179 ± 66	396 ± 93	14 ± 19
G10	8.8 ± 0.8	1.056 ± 0.141	15.4 ± 0.9	20 ± 15	2.23 ± 0.93	0.87 ± 2.05	12.1 ± 1.1	4.6 ± 1.5	70 ± 14	158 ± 27	33 ± 4	70 ± 14	187 ± 40	345 ± 116	62 ± 67
G11	8.9 ± 0.8	0.943 ± 0.261	15.0 ± 1.5	273 ± 551	3.84 ± 2.12	0.23 ± 0.50	10.8 ± 2.6	3.8 ± 0.8	65 ± 17	143 ± 45	37 ± 12	65 ± 17	147 ± 56	305 ± 113	65 ± 70
W1	7.4 ± 0.4	0.937 ± 0.208	16.8 ± 4.1	11 ± 6	8.32 ± 5.92	0.60 ± 0.79	96.8 ± 25.8	19.3 ± 4.5	13 ± 12	58 ± 14	134 ± 36	13 ± 12	65 ± 15	267 ± 81	3 ± 7
W2	7.7 ± 0.6	0.923 ± 0.197	17.1 ± 4.6	81 ± 140	8.10 ± 2.99	8.86 ± 20.74	84.9 ± 21.7	22.6 ± 6.1	22 ± 21	69 ± 14	104 ± 24	22 ± 21	72 ± 12	311 ± 85	43 ± 109
W3	8.3 ± 1.2	1.169 ± 0.201	17.1 ± 4.4	184 ± 263	6.36 ± 3.51	26.23 ± 20.13	58.6 ± 36.1	13.6 ± 6.2	14 ± 21	108 ± 65	76 ± 28	14 ± 21	150 ± 136	429 ± 157	24 ± 35
A	7.4 ± 0.3	0.967 ± 0.175	14.5 ± 2.2	488 ± 473	5.19 ± 1.84	4.36 ± 2.53	47.8 ± 19.1	11.8 ± 3.6	25 ± 13	110 ± 23	75 ± 24	25 ± 13	131 ± 30	351 ± 99	1 ± 1

S2.7 Wastewater treatment plant (WWTP) contribution

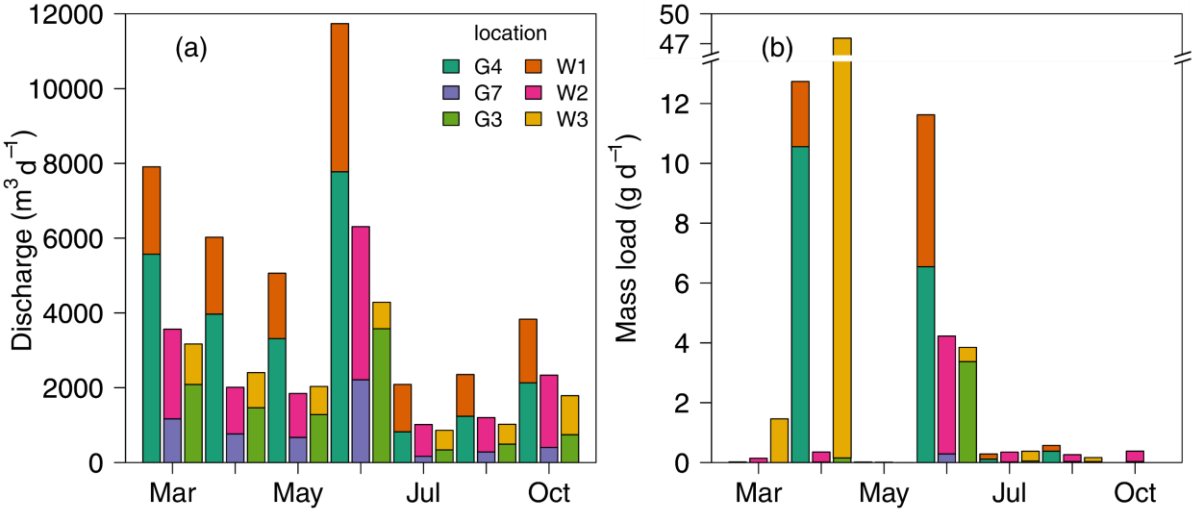

Figure S6: Contribution of river and WWTPs to the total reach discharge (a) and associated *S*-metolachlor loads (b) for monthly sampling. G4, G7 and G3 were located directly upstream of the effluents of WWTPs 1, 2 and 3, respectively. Note that G4 is downstream of G3, and W3 thus contributed to the G4 discharge.

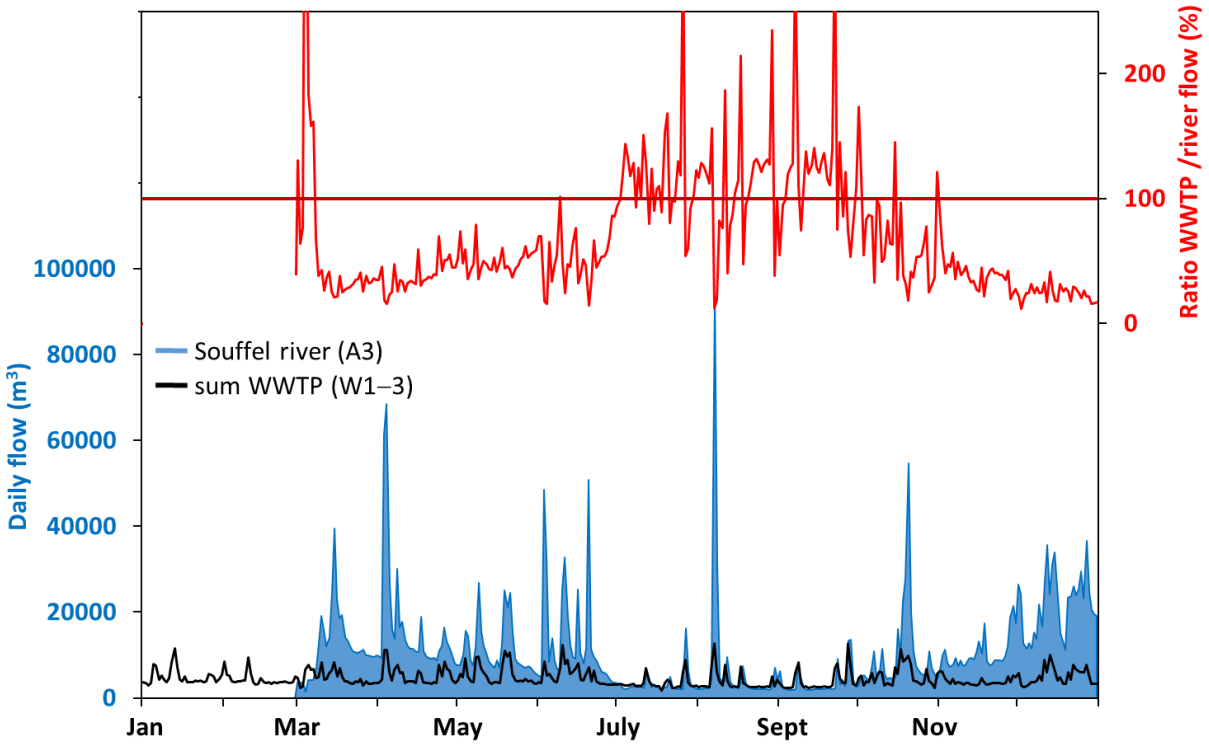

Figure S7: Daily flow in 2019 at the catchment outlet (A3) and sum of the wastewater treatment plant (WWTP) outflow. Ratio between the two flows higher than 100% indicates when the flow at A3 was lower than the sum of WWTP flow, indicating uptake by riparian vegetation and infiltration from the river into groundwater through the hyporheic zone.

S2.8 *S*-metolachlor transformation products

Table S12: Contributions of three *S*-metolachlor transformation products (metolachlor ethane sulfonic acid (ESA), metolachlor oxanilic acid (OXA) and metolachlor NOA 413173) to the total concentration of *S*-metolachlor and its transformation products (expressed as molar equivalents of *S*-metolachlor) across eight monthly monitoring stations of the Rhin-Meuse Water Agency in 2019. Data are presented as means ± standard deviation per month, per season (Spring: A-M-J; Summer: J-A-S; Fall: O-N-D and winter: J-F-M) and for the 2019 year (Dataset available on https://naiades.eaufrance.fr/donnees-disponibles).

Month (2019)	%SM/MEL$_{SM}$	%TPS/MEL$_{SM}$	%ESA/MEL$_{SM}$*	%OXA/MEL$_{SM}$*	%SM/MEL$_{SM}$*	(%ESA + %OXA) / %TPS
January (n= 8)	6.6 ± 3 %	93.4 ± 3 %	70.7 ± 11.8 %	17 ± 6.7 %	12.3 ± 6 %	51.2 ± 8.8 %
February (n = 8)	2.5 ± 1.5 %	97.5 ± 1.5 %	80.6 ± 4.2 %	15.2 ± 2 %	4.3 ± 2.4 %	56.8 ± 5 %
March (n = 8)	4.3 ± 2.8 %	95.7 ± 2.8 %	79.1 ± 5.9 %	13.8 ± 1.6 %	7.1 ± 4.5 %	57.6 ± 2.6 %
April (n = 7)	42.1 ± 29.4 %	57.9 ± 29.4 %	39.9 ± 27 %	10.2 ± 5.4 %	50 ± 31.6 %	61.3 ± 4.6 %
May (n = 11)	56.2 ± 34.9 %	43.8 ± 34.9 %	30.5 ± 30.3 %	6.2 ± 4.6 %	63.3 ± 33.7 %	62.8 ± 13.9 %
June (n = 8)	30.9 ± 16.6 %	69.1 ± 16.6 %	51 ± 16.7 %	10.1 ± 2.1 %	38.8 ± 15.6 %	67.3 ± 13.7 %
July (n = 6)	21.4 ± 24.7 %	78.6 ± 24.7 %	56.1 ± 31.3 %	14.5 ± 4.8 %	29.4 ± 31.6 %	54.8 ± 15.1 %
August (n = 3)	16 ± 18.5 %	84 ± 18.5 %	53.8 ± 46.9 %	17.9 ± 12.1 %	28.3 ± 34.9 %	51.4 ± 20.8 %
September (n = 7)	10.7 ± 8.4 %	89.3 ± 8.4 %	38 ± 47.4 %	37.5 ± 29.5 %	24.5 ± 20.9 %	42 ± 15.5 %
October (n = 7)	13.8 ± 8.1 %	86.2 ± 8.1 %	60.7 ± 10.8 %	20.6 ± 5.3 %	18.7 ± 9.4 %	67.9 ± 7.5 %
November (n =7)	7.1 ± 3.6 %	92.9 ± 3.6 %	75.6 ± 7 %	14.4 ± 3.2 %	10 ± 4.7 %	67.6 ± 4.3 %
December (n = 7)	19.2 ± 11.8 %	80.8 ± 11.8 %	56.8 ± 12.3 %	16.7 ± 4.4 %	26.5 ± 14 %	62.5 ± 5.3 %
Spring (n = 26)	44.6 ± 29.9 %	55.4 ± 29.9 %	39.3 ± 26.4 %	8.5 ± 4.5 %	52.2 ± 29.6 %	63.8 ± 11.9 %
Summer (n = 16)	15.7 ± 17.4 %	84.3 ± 17.4 %	47.8 ± 40 %	25.2 ± 22.4 %	27 ± 26 %	48.5 ± 16.3 %
Fall (n = 22)	13.6 ± 9.7 %	86.4 ± 9.7 %	64 ± 12.9 %	17.2 ± 4.9 %	18.8 ± 12.1 %	65.8 ± 6.1 %
Winter (n = 24)	4.4 ± 2.9 %	95.6 ± 2.9 %	76.8 ± 8.8 %	15.3 ± 4.2 %	7.9 ± 5.5 %	55.2 ± 6.5 %
Year (n = 88)	20.7 ± 24.4 %	79.3 ± 24.4 %	57.2 ± 27.7 %	15.6 ± 11.7 %	27.2 ± 26.8 %	59.2 ± 12.2 %

MEL$_{SM}$ is calculated with equation S1 with ESA, OXA and NOA, and only with ESA and OXA for MEL$_{SM}$* to be comparable to Rose et al. (2018)

$$MEL_{SM} = load(SM) + \sum_{i=1}^{TPs} load(TP_i) \times \frac{MW_{SM}}{MW_{TP_i}} \quad \text{(S1)}$$

where MW_{SM} and MW_{TPi} correspond to the molar weight of *S*-metolachlor, and that of its TPs, respectively. The proportion of each TPs, i.e. %ESA, %OXA and %NOA, can be expressed as the ratio of the associated mass equivalent loads on the MEL$_{SM}$ or the MEL$_{SM}$*.

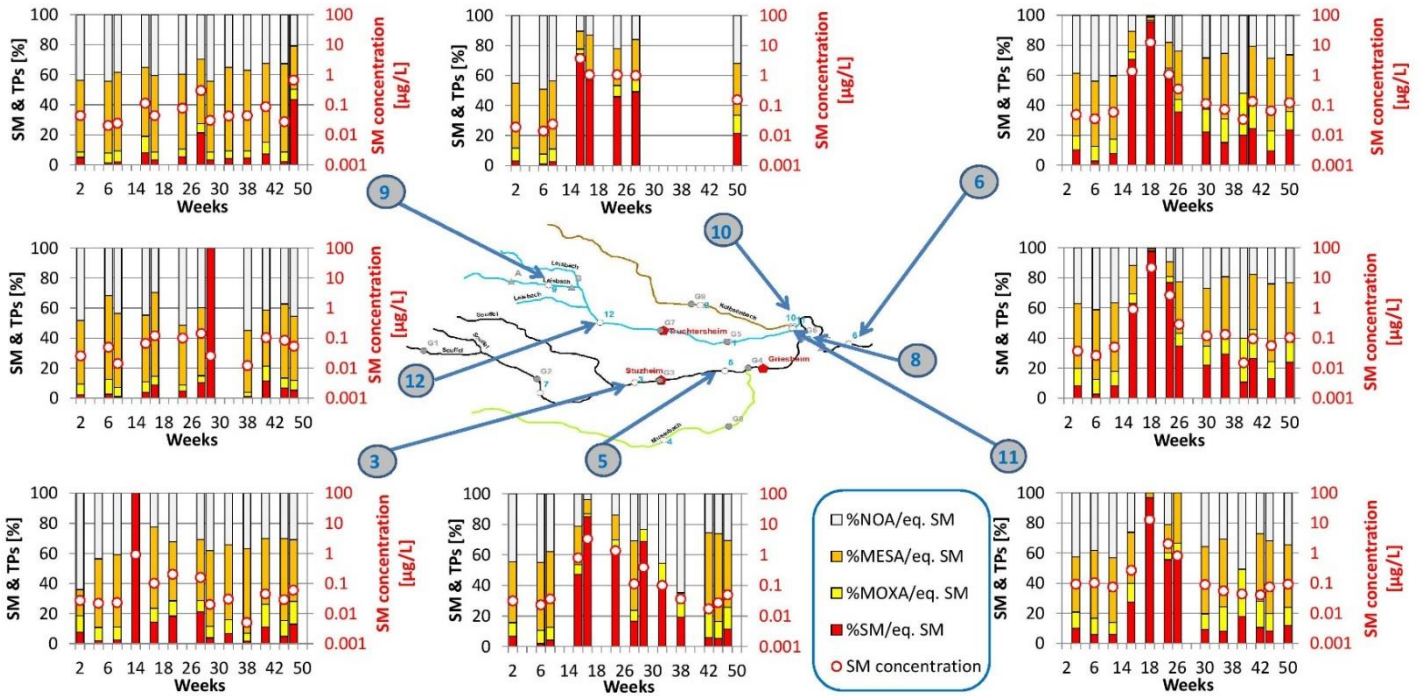

Figure S8: *S*-metolachlor concentrations at the eight monthly monitoring stations of the Rhin-Meuse Water Agency in 2019 are presented on a logarithmic scale (0.001 to 100 µg/L) using the secondary y-axis on the right side of each graph. These concentrations are depicted as red circles with white fill. The relative contributions of three transformation products - metolachlor ethane sulfonic acid (ESA), metolachlor oxanilic acid (OXA), and metolachlor NOA 413173 - to the total concentration (*S*-metolachlor plus transformation products, expressed in molar equivalents of *S*-metolachlor) are shown on the secondary y-axis on the left side of each graph.

Table S13: Analytical method description for the transformation products of S-metolachlor (ISO/IEC 17025-accredited laboratory - Eurofins Hydrologie Est, COFRAC).

Parameters	Quantification limit (µg/L)	Uncertainty method	Extraction method*	Separation method	Detection method	Analytical method
S-metolachlor ESA	0.01	NF ISO 11352	SPE	HPLC	MS/MS	Internal method
S-metolachlor OXA	0.005	NF ISO 11352	SPE	HPLC	MS/MS	Internal method
S-metolachlor NOA 413173	0.02	NF ISO 11352	SPE	HPLC	MS/MS	Internal method
S-metolachlor	0.005	NF ISO 11352	LLE	HPLC	MS/MS	Internal method

340 * SPE: Solid-Phase Extraction; LLE: Liquid-Liquid Extraction

S3 Supplement references

Akan, A. O.: 3-Normal flow, in: Open Channel Hydraulics, edited by: Akan, A. O., Butterworth-Heinemann, Oxford, 67–96, 2006.

Ali, G., Birkel, C., Tetzlaff, D., Soulsby, C., McDonnell, J. J., and Tarolli, P.: A comparison of wetness indices for the prediction of observed connected saturated areas under contrasting conditions, Earth Surf. Proc. Land., 39, 399–413, https://doi.org/10.1002/esp.3506, 2014.

Alvarez-Zaldívar, P., Payraudeau, S., Meite, F., Masbou, J., and Imfeld, G.: Pesticide degradation and export losses at the catchment scale: Insights from compound-specific isotope analysis (CSIA), Water Res., 139, 198–207, https://doi.org/10.1016/j.watres.2018.03.061, 2018.

Bauer-Marschallinger, B., Paulik, C., Hochstoger, S., Mistelbauer, T., Modanesi, S., Ciabatta, L., Massari, C., Brocca, L., and Wagner, W.: Soil moisture from fusion of scatterometer and SAR: Closing the scale gap with temporal filtering, Remote Sensing, 10, 1030, https://doi.org/10.3390/rs10071030, 2018.

Boesten, J. and Linden, A.: Modeling the influence of sorption and transformation on pesticide leaching and persistence, Journal of Environment Quality, 20, 425–435, https://doi.org/10.2134/jeq1991.00472425002000020015x, 1991.

Davie-Martin, C. L., Hageman, K. J., and Chin, Y.-P.: An improved screening tool for predicting volatilization of pesticides applied to soils, Environ. Sci. Technol., 47, 868–876, https://doi.org/10.1021/es3020277, 2013.

Drouin, G., Droz, B., Leresche, F., Payraudeau, S., Masbou, J., and Imfeld, G.: Direct and indirect photodegradation of atrazine and *S*-metolachlor in agriculturally impacted surface water and associated C and N isotope fractionation, Environ. Sci. Process. Impacts, 23, 1791–1802, https://doi.org/10.1039/D1EM00246E, 2021.

Droz, B., Drouin, G., Lohmann, J., Guyot, B., Payraudeau, S., and Imfeld, G.: Data for "How multi-scale monitoring in catchment area combined to compound-specific isotope analysis approach can reveal *S*-metolachlor degradation?" (v1.0), Zenodo [dataset], https://doi.org/10.5281/zenodo.6414880, 2024.

Droz, B., Drouin, G., Maurer, L., Villette, C., Payraudeau, S., and Imfeld, G.: Phase transfer and biodegradation of pesticides in water-sediment systems explored by compound-specific isotope analysis and conceptual modeling, Environ. Sci. Technol., 55, 4720–4728, https://doi.org/10.1021/acs.est.0c06283, 2021.

Fono, L. J., Kolodziej, E. P., and Sedlak, D. L.: Attenuation of wastewater-derived contaminants in an effluent-dominated river, Environ. Sci. Technol., 40, 7257–7262, https://doi.org/10.1021/es061308e, 2006.

Fox, G. A., Pulijala, S. H., and Sabbagh, G. J.: Influence of rainfall distribution on simulations of atrazine, metolachlor, and isoxaflutole/metabolite transport in subsurface drained fields, J. Agric. Food Chem., 55, 5399–5407, https://doi.org/10.1021/jf063753z, 2007.

Gish, T. J., Prueger, J. H., Daughtry, C. S. T., Kustas, W. P., McKee, L. G., Russ, A. L., and Hatfield, J. L.: Comparison of field-scale herbicide runoff and volatilization losses: An eight-year field investigation, J. Environ. Qual., 40, 1432–1442, https://doi.org/10.2134/jeq2010.0092, 2011.

Habets, F., Boone, A., Champeaux, J. L., Etchevers, P., Franchistéguy, L., Leblois, E., Ledoux, E., Le Moigne, P., Martin, E., Morel, S., Noilhan, J., Quintana Seguí, P., Rousset-Regimbeau, F., and Viennot, P.: The SAFRAN-ISBA-MODCOU hydrometeorological model applied over France, Journal of Geophysical Research: Atmospheres, 113, D06113, https://doi.org/10.1029/2007jd008548, 2008.

Hengl, T., Mendes de Jesus, J., Heuvelink, G. B. M., Ruiperez Gonzalez, M., Kilibarda, M., Blagotić, A., Shangguan, W., Wright, M. N., Geng, X., Bauer-Marschallinger, B., Guevara, M. A., Vargas, R., MacMillan, R. A., Batjes, N. H., Leenaars, J. G. B., Ribeiro, E., Wheeler, I., Mantel, S., and Kempen, B.: SoilGrids250m: Global gridded soil information based on machine learning, PLoS One, 12, e0169748, https://doi.org/10.1371/journal.pone.0169748, 2017.

Hippelein, M. and McLachlan, M. S.: Soil/air partitioning of semivolatile organic compounds. 2. Influence of temperature and relative humidity, Environ. Sci. Technol., 34, 3521–3526, https://doi.org/10.1021/es991421n, 2000.

Huang, L. Q. and Frink, C. R.: Distribution of atrazine, simazine, alachlor, and metolachlor in soil profiles in Connecticut, Bull. Environ. Contam. Toxicol., 43, 159–164, https://doi.org/10.1007/BF01702253, 1989.

Jaikaew, P., Malhat, F., Boulange, J., and Watanabe, H.: Aspect of the degradation and adsorption kinetics of atrazine and metolachlor in andisol soil, Hellenic Plant Protection Journal, 10, 1–14, https://doi.org/10.1515/hppj-2017-0001, 2017.

Kronvang, B., Strøm, H., Hoffmann, C. C., Laubel, A., and Friberg, N.: Subsurface tile drainage loss of modern pesticides: field experiment results, Water Sci. Technol., 49, 139–147, https://doi.org/10.2166/wst.2004.0181, 2004.

Lefrancq, M., Van Dijk, P., Jetten, V., Schwob, M., and Payraudeau, S.: Improving runoff prediction using agronomical information in a cropped, loess covered catchment, Hydrol. Process., 31, 1408–1423, https://doi.org/10.1002/hyp.11115, 2017.

Leifer, A.: The kinetics of environmental aquatic photochemistry: Theory and practice, American Chemical Society, 336 pp.1988.

Lemke, D., Liao, Z., Wöhling, T., Osenbrück, K., and Cirpka, O. A.: Concurrent conservative and reactive tracer tests in a stream undergoing hyporheic exchange, Water Resour. Res., 49, 3024-3037, https://doi.org/10.1002/wrcr.20277, 2013.

Liao, Z., Lemke, D., Osenbrück, K., and Cirpka, O. A.: Modeling and inverting reactive stream tracers undergoing two-site sorption and decay in the hyporheic zone, Water Resour. Res., 49, 3406–3422, https://doi.org/10.1002/wrcr.20276, 2013.

Payraudeau, S., Alvarez-Zaldivar, P., van Dijk, P., and Imfeld, G.: Constraining pesticide degradation in conceptual distributed catchment models with compound-specific isotope analysis (CSIA), EGUsphere, 2024, 1–28, https://doi.org/10.5194/egusphere-2024-2840, 2024.

Prueger, J. H., Gish, T. J., McConnell, L. L., McKee, L. G., Hatfield, J. L., and Kustas, W. P.: Solar radiation, relative humidity, and soil water effects on metolachlor volatilization, Environ. Sci. Technol., 39, 5219–5226, https://doi.org/10.1021/es048341q, 2005.

Ramnarine, R., Voroney, R. P., Wagner-Riddle, C., and Dunfield, K. E.: Carbonate removal by acid fumigation for measuring the $\delta^{13}C$ of soil organic carbon, Can. J. Soil Sci., 91, 247–250, https://doi.org/10.4141/cjss10066, 2011.

Rice, P. J., Anderson, T. A., and Coats, J. R.: Degradation and persistence of metolachlor in soil: Effects of concentration, soil moisture, soil depth, and sterilization, Environ. Toxicol. Chem., 21, 2640–2648, https://doi.org/10.1002/etc.5620211216, 2002.

Rose, C. E., Coupe, R. H., Capel, P. D., and Webb, R. M. T.: Holistic assessment of occurrence and fate of metolachlor within environmental compartments of agricultural watersheds, Sci. Total Environ., 612, 708–719, https://doi.org/10.1016/j.scitotenv.2017.08.154, 2018.

Salehin, M., Packman, A. I., and Wörman, A.: Comparison of transient storage in vegetated and unvegetated reaches of a small agricultural stream in Sweden: seasonal variation and anthropogenic manipulation, Adv. Water Resour., 26, 951-964, https://doi.org/10.1016/s0309-1708(03)00084-8, 2003.

Schwarzenbach, R. P., Gschwend, P. M., and Imboden, D. M.: Environmental organic chemistry, third ed., John Wiley & Sons, 1024 pp.2016.

Shaw, S. B., Beslity, J. O., and Colvin, M. E.: Working toward a more holistic set of hydrologic principles to teach non-hydrologists: Five simple concepts within catchment hydrology, Hydrol. Process., 33, 2258–2262, https://doi.org/10.1002/hyp.13485, 2019.

Si, Y., Takagi, K., Iwasaki, A., and Zhou, D.: Adsorption, desorption and dissipation of metolachlor in surface and subsurface soils, Pest Manage. Sci., 65, 956–962, https://doi.org/10.1002/ps.1779, 2009.

Silva, V., Mol, H. G. J., Zomer, P., Tienstra, M., Ritsema, C. J., and Geissen, V.: Pesticide residues in European agricultural soils – A hidden reality unfolded, Sci. Total Environ., 653, 1532–1545, https://doi.org/10.1016/j.scitotenv.2018.10.441, 2019.

Van Breukelen, B. M.: Quantifying the degradation and dilution contribution to natural attenuation of contaminants by means of an open system Rayleigh equation, Environ. Sci. Technol., 41, 4980–4985, https://doi.org/10.1021/es062846u, 2007.

Walker, A.: A simulation model for prediction of herbicide persistence, J. Environ. Qual., 3, 396–401, https://doi.org/10.2134/jeq1974.00472425000300040021x, 1974.